JOURNAL OF VIROLOGY, Nov. 2007, p. 12406–12417 Vol. 81, No. 22
0022-538X/07/$08.00+0 doi:10.1128/JVI.01107-07

Virus-Encoded Aminoacyl-tRNA Synthetases: Structural and Functional Characterization of Mimivirus TyrRS and MetRS[▽]

Chantal Abergel,[1]* Joëlle Rudinger-Thirion,[2] Richard Giegé,[2] and Jean-Michel Claverie[1]

Structural and Genomic Information Laboratory, CNRS-UPR2589, Institut de Biologie Structurale & Microbiologie IFR88, Université de la Méditerranée, 163 avenue de Luminy, Case 934, 13288 Marseille, Cedex 9, France,[1] and Architecture et Réactivité de l'ARN, CNRS-UPR 9002, IBMC, and Université Louis Pasteur, 15 rue René Descartes, 67084 Strasbourg, France[2]

Received 22 May 2007/Accepted 4 September 2007

Aminoacyl-tRNA synthetases are pivotal in determining how the genetic code is translated in amino acids and in providing the substrate for protein synthesis. As such, they fulfill a key role in a process universally conserved in all cellular organisms from their most complex to their most reduced parasitic forms. In contrast, even complex viruses were not found to encode much translation machinery, with the exception of isolated components such as tRNAs. In this context, the discovery of four aminoacyl-tRNA synthetases encoded in the genome of mimivirus together with a full set of translation initiation, elongation, and termination factors appeared to blur what was once a clear frontier between the cellular and viral world. Functional studies of two mimivirus tRNA synthetases confirmed the MetRS specificity for methionine and the TyrRS specificity for tyrosine and conformity with the identity rules for $tRNA^{Tyr}$ for archea/eukarya. The atomic structure of the mimivirus tyrosyl-tRNA synthetase in complex with tyrosinol exhibits the typical fold and active-site organization of archaeal-type TyrRS. However, the viral enzyme presents a unique dimeric conformation and significant differences in its anticodon binding site. The present work suggests that mimivirus aminoacyl-tRNA synthetases function as regular translation enzymes in infected amoebas. Their phylogenetic classification does not suggest that they have been acquired recently by horizontal gene transfer from a cellular host but rather militates in favor of an intricate evolutionary relationship between large DNA viruses and ancestral eukaryotes.

Acanthamoeba polyphaga mimivirus is the largest known DNA virus. Its particle size (750 nm), genome length (1.2 million bp), and large gene repertoire (>910 protein-coding genes) blur the established boundaries between viruses and parasitic cellular organisms (49). On the one hand, mimivirus exhibits the standard features of nucleocytoplasmic large DNA viruses (capsid structure, life cycle, and core gene set), within which it now constitutes the prototype of the *Mimiviridae* family besides the previously defined *Poxviridae*, *Asfarviridae*, *Iridoviridae*, and *Phycodnaviridae* families (49). On the other hand, the mimivirus genome exhibits numerous genes never encountered before in any other virus. Among the most intriguing are genes corresponding to central components of the protein translation machinery, a biochemical process widely thought to be an exclusive signature of cellular organisms. For instance, the mimivirus genome encodes four aminoacyl-tRNA synthetases (aaRS): ArgRS, CysRS, MetRS, and TyrRS. These key enzymes link the genetic code with the proper 20 amino acids and provide the basic substrates for the translation process. In cellular organisms, they catalyze the esterification of a given amino acid to the 3′ ends of their cognate tRNAs in a two-step reaction comprising the activation of the amino acid as an aminoacyl-adenylate followed by its transfer onto the 3′-terminal ribose of the cognate tRNA (13). The correct interpretation of the genetic code thus requires a perfect specificity at both the amino acid activation and the tRNA-charging step. The specificity of the tRNA recognition is ensured by stringent constraints referred to as "identity rules" (30). aaRS are structurally diverse enzymes with modular architectures, traditionally partitioned into two classes based on signature sequences and common features of their catalytic sites (17, 23). Class I aaRS share the sequence motifs HIGH and KMSKS and have active sites based on a Rossmann-fold domain. Class II aaRS share three other signature motifs, and their active sites are built on an antiparallel β-sheet surrounded by α-helices. There are also functional differences between the two classes: class I aaRS attach amino acids to the 2′-hydroxyl end of the terminal adenosine of the tRNA, whereas charging occurs on the 3′-hydroxyl end for class II aaRS (5). Tyrosyl-tRNA synthetases belong to class Ic of aaRS, together with TrpRS. Both are homodimers (18), a feature otherwise shared mostly by class II synthetases.

Two main opposite hypotheses can be proposed to account for the presence of the largely incomplete translation machinery exhibited by mimivirus. Either it is the remnant of a complete translation machinery, following many gene losses through a process of reductive evolution (such as observed for intracellular parasitic bacteria), or it is the result of multiple horizontal gene acquisitions conferring some selective advantages to the virus. The latter is most often accomplished by diverting the acquired genes from their original functions. To address the above-mentioned dilemma, we initiated a comprehensive study of the structures and activities of the four mimivirus class I aaRS. We complemented these experimental stud-

* Corresponding author. Mailing address: Structural and Genomic Information Laboratory, CNRS-UPR2589, IBSM-IFR88, 163 avenue de Luminy, Case 934, 13288 Marseille, Cedex 9, France. Phone: (33) 491 825422. Fax: (33) 491 825421. E-mail: Chantal.Abergel@igs.cnrs-mrs.fr.

▽ Published ahead of print on 12 September 2007.

ies by searching for evidence of horizontal gene transfers through a phylogenetic analysis of the four mimivirus aaRS.

This article reports a detailed functional study of two of the four viral class I aaRS, *A. polyphaga* mimivirus TyrRS ($TyrRS_{apm}$) and *A. polyphaga* mimivirus MetRS ($MetRS_{apm}$), and the structural study of $TyrRS_{apm}$ in complex with tyrosinol. These enzymes were found to exhibit the specificity and function predicted from their sequences, but the three-dimensional structure of $TyrRS_{apm}$ exhibited significant differences from its cellular counterparts.

Phylogenetic analysis did not provide evidence for a recent acquisition of these genes from a cellular host close to modern *Acanthamoeba* but connected mimivirus aaRS to a variety of early diverging protozoan supergroups, such as Amoebozoa and Excavata (3).

MATERIALS AND METHODS

Preparation of $TyrRS_{apm}$, $MetRS_{apm}$, and tRNAs. The *A. polyphaga* mimivirus TyrRS-encoding gene was PCR amplified from genomic DNA and cloned into a Gateway system (Invitrogen) (33) as described earlier (1, 2).

The oligomeric state of recombinant TyrRS was measured by gel filtration on an analytical S200 column. Purified TyrRS was loaded on the column at a 10-mg/ml concentration in 10 mM Tris buffer (pH 7.4), 100 mM KCl. Five molecular weight standards were initially run onto the column, using the same buffer to calibrate the column.

Native $tRNA^{Tyr}$ and initiator $tRNA^{Met}$ from *Escherichia coli* were purchased from Subriden and Sigma, respectively. Their equivalents in *Saccharomyces cerevisiae* were purified to homogeneity by countercurrent distribution (21) followed by appropriate column chromatographies. Transcripts of yeast $tRNA^{Tyr}$ and initiator $tRNA^{Met}$ as well as their variants were obtained as described elsewhere (19, 26). Finally, transcripts of *Plasmodium falciparum* $tRNA^{Tyr}$ were obtained by in vitro transcription of synthetic genes using the "transzyme" method (25).

Crystallization and structure determination of $TyrRS_{apm}$. The selenomethionyl substituted protein was produced using a standard protocol (34). Crystallization was improved by introducing anion-exchange chromatography (Aktä Explorer 10S; GE Healthcare) on a Resource Q column (6 ml) using an NaCl gradient (0 to 1 M, 20 column volume). Three fractions were recovered (150 mM, 200 mM, and 240 mM NaCl), and the best crystals were obtained with the second fraction desalted in 20 mM Tris (pH 7.4) and concentrated to 14 mg/ml. The crystals were grown at 298 K by vapor diffusion mixing 2 μl of TyrRS solution containing tyrosinol and ATP, 1 mM, with 0.5 μl of reservoir (500 μl) 0.1 M sodium citrate (pH 5.5) and 6 to 9% polyethylene glycol 4000 (wt/vol), 15% 2-methyl-2, 4-pentane-d_{12}-diol, 0.1 M KCl, 1 mM $MgCl_2$. Crystals belong to the orthorhombic space group $P2_12_12_1$ (a = 63.25, b = 107.19, c = 148.67 Å), with one biological dimer per asymmetric unit. Both multiwavelength anomalous diffraction and native datasets were collected at the European Synchrotron Radiation Facility synchrotron beamline ID29 and integrated using MOSFLM (40). Data were scaled and reduced using the CCP4i package (16, 24) (Table 1).

Even though selenomethionyl substituted protein crystals produced low-resolution data and were fast decaying under X-ray exposure, a full 4-Å-resolution multiwavelength anomalous diffraction data set was collected. AutoSHARP (10) was used to obtain initial phases, 23 selenium atoms were located and refined, and solvent flattening was performed to improved phases. The resulting electronic density map was used to superimpose in TURBO-FRODO (50) a model of the TyrRS structure produced using MODELLER (51) onto the refined selenium atom positions. A round of manual building was performed to better fit the initial model in the electronic density map and to remove the portions of the model that were not in density.

The unrefined structure was then used to identify a molecular replacement solution (AMoRe [43]) with a 2.2-Å data set of native TyrRS protein in complex with tyrosinol and ATP. The model was refined further by using rigid body refinement followed by several rounds of positional refinement in CNS (11), with manual rebuilding using TURBO-FRODO (50). The quality of the structure was assessed using PROCHECK (39) (Table 1).

Buried surface area computations were performed using GRASP (44). The detailed calculation for the various TyrRS dimer conformations required the modeling of a 20-residue connective polypeptide 1 (CP1) region next to the α_6-turn-α_7 motif, structurally conserved in all TyrRSs but disordered in the $TyrRS_{apm}$ structure (see Fig. 3). This region was not found to contribute significantly to the difference of buried surface areas between the two $TyrRS_{apm}$ dimer conformations. Structure graphical representations (see Fig. 2 and 4 to 6) were produced using VMD (35).

TABLE 1. X-ray data collection and refinement statistics

Parameter	Value or type[a]
Data collection	
Beam line	ESRF/ID29
Wavelength (Å)	0.97925
Space group	$P2_12_12_1$
Unit cell dimensions (Å)	a = 63.5, b = 107.3, c = 148.9
Resolution range (Å)	87.7 to 2.2 (2.28 to 2.2)
No. of observations	238,357
No. of unique reflections	52,537
Multiplicity	4.5 (4.6)
Completeness (%)	100 (100)
$<I/\sigma I>$[b]	2.2 (2.3)
R_{sym} (%)[c]	9.1 (28.9)
Refinement	
Resolution range (Å)	29.8 to 2.2
R_{cryst} (%)[d]	21.6
R_{free} (%)[e]	24.8
Δ_{bond} (Å)	0.006
Δ_{angle} (°)	1.1
No. of protein atoms	5,169
No. of water molecules	330
Ligand tyrosinol	2
Average B factor (Å^2)	39
Protein main chain	37.1
Water	41.85
Ramachandran plot (%)	
Most favored regions	539
Allowed regions	40
Generously allowed regions	5
Disallowed regions	0

[a] Values in parentheses are for the highest-resolution shell.

[b] $<I/\sigma I>$ is the mean signal-to-noise ratio, where I is the integrated intensity of a measured reflection and σ is the estimated error in the measurement.

[c] $R_{sym} = \Sigma_h\Sigma_i|I_{h,i} - \langle I_h\rangle|/\Sigma_h\Sigma_i I_{h,i}$, where I is the integrated intensity of reflection h having i observations and $\langle I_h\rangle$ is the mean recorded intensity of reflection h over multiple recordings.

[d] $R_{cryst} = \Sigma||F_o|-|F_c||/\Sigma|F_o|$, where F_o and F_c are observed and calculated structure factor amplitudes, respectively.

[e] R_{free} was calculated from a randomly chosen 5% of reflections.

Activity assays. (i) ATP/PP_i exchange reactions. Reaction media (200 μl) contained 100 mM Na-HEPES (pH 7.2), 10 mM $MgCl_2$, 2 mM KF, 2 mM ATP, 2 mM [^{32}P]PP_i (1 to 2 cpm/pmol), and 1 mM of a mixture of all amino acids, with or without tyrosine or methionine. Reactions were initiated by addition of 1.5 μg of $TyrRS_{apm}$ or $MetRS_{apm}$. The levels of [^{32}P]ATP formed after 5, 10, 15, and 20 min of incubation at 37°C were determined as described elsewhere (12). Control experiments with either no aaRS or no amino acid were conducted in parallel.

(ii) $tRNA^{Tyr}$ aminoacylation reactions. Before aminoacylation, the eluted transcripts were heated at 65°C for 2 min and cooled for 10 min to allow native conformation. Tyrosylation of native $tRNA^{Tyr}$ or $tRNA^{Tyr}$ transcripts (wild type or mutated) was performed (50 μl) at 30°C in 50 mM Na-HEPES (pH 7.5), 25 mM KCl, 12 mM $MgCl_2$, 2.5 mM ATP, 0.2 mg/ml bovine serum albumin, 1 mM spermine (54), 10 μM L-[^{14}C]tyrosine (adjusted to 750 cpm/pmol), and the required concentration of tRNA molecules and $TyrRS_{apm}$. Methionylation of initiator $tRNA^{Met}$ or $tRNA^{Met}$ transcripts (wild type or mutated) was performed (50 μl) at 30°C in 20 mM Na-HEPES (pH 7.5), 10 mM $MgCl_2$, 1 mM dithioerythritol, 2 mM ATP (4), 10 μM L-[^{35}S]methionine (adjusted to 400 cpm/pmol), and the required concentration of tRNA molecules and $MetRS_{apm}$. At different incubation times, aliquots were spotted on 3MM Whatman paper and 5% trichloroacetic acid precipitated. Incorporation of radioactive amino acid was measured by liquid scintillation spectroscopy. Kinetic parameters (K_m and k_{cat}) were determined from Lineweaver and Burk plots.

Phylogenetic position of mimivirus aaRS. Homologous TyrRS protein sequences from all major phyla were aligned using MUSCLE software (22), and a maximum-likelihood tree was computed with PhyML (32) using the default

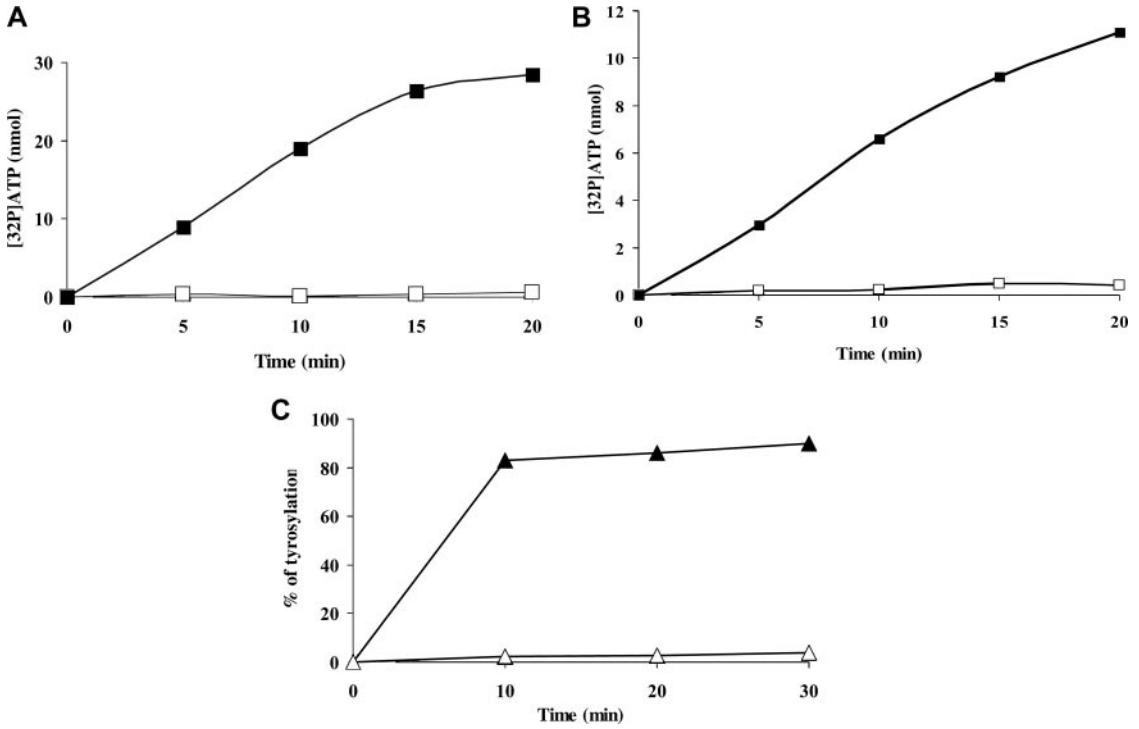

FIG. 1. Functional assays of $TyrRS_{apm}$ and $MetRS_{apm}$. Amino acid activation of $TyrRS_{apm}$ and $MetRS_{apm}$. Reactions were conducted in the presence of a mix of all amino acids minus (□) or plus (■) tyrosine (A) or methionine (B). (C) Tyrosylation of *E. coli* (△) and yeast (▲) native $tRNA^{Tyr}$ by $TyrRS_{apm}$. Enzyme and tRNA concentrations were 20 μM and 1.3 μM, respectively.

option on our phylogeny server at the URL http://www.phylogeny.fr/. Bootstrap values are indicated along the branches. Branches have been collapsed for bootstrap values smaller than 50%.

Additional phylogenetic analyses of all four mimivirus aaRS were performed using archeal and eukaryotic aaRS, including mitochondrial sequences (bacterial-type aaRS). For each aaRS, protein sequences were aligned using T-Coffee software (45). Maximum-likelihood trees and neighbor-joining trees (Bootstrap 500) were computed as described above. The two methods produced similar trees. Only maximum-likelihood trees are presented in Fig. 7.

Protein structure accession number. The $TyrRS_{apm}$ structure coordinates have been deposited in the Protein Data Bank under accession code 2J5B.

RESULTS AND DISCUSSION

$TyrRS_{apm}$ and $MetRS_{apm}$ possess the predicted enzymatic activities. The presence of aaRS genes in a viral genome was unexpected and immediately raised the question of the activity of the corresponding protein. We expressed and purified two of the four mimivirus aaRS (MetRS, TyrRS, ArgRS, and CysRS), namely, $MetRS_{apm}$ and $TyrRS_{apm}$. They were both tested for amino acid activation activity in the absence of tRNA (2, 49). Exchange reactions were assayed in the presence of TyrRS and all amino acids with or without tyrosine (Fig. 1A) and in the presence of MetRS and all amino acids with or without methionine (Fig. 1B). These experiments clearly demonstrate that $TyrRS_{apm}$ and $MetRS_{apm}$ indeed activate tyrosine and methionine, respectively, to the exclusion of any other amino acid. Furthermore, $TyrRS_{apm}$ specifically tyrosylates $tRNA^{Tyr}$, while $MetRS_{apm}$, as other methionyl-tRNA synthetases, aminoacylates both eukaryotic and bacterial $tRNA^{Met}$ (Fig. 1C; Table 2).

Structure of $TyrRS_{apm}$. (i) The overall structure of $TyrRS_{apm}$ resembles that of other TyrRSs. TyrRSs are all organized similarly, with an N-terminal catalytic domain, including the CP1 region responsible for dimerization, followed by a C-terminal domain (8). However, TyrRSs do exhibit important differences in sequence and architecture of their C-terminal domains. Archaeal TyrRSs are encoded by the shortest polypeptides, whereas vertebrate TyrRSs exhibit a large extra C-terminal domain. For the human cytoplasmic TyrRS and *Neurospora crassa* mitochondrial TyrRS, these differences have been associated with functions unrelated to the translation process (14, 59).

As expected from its sequence similarity to other TyrRSs, $TyrRS_{apm}$ exhibits the typical fold of the TyrRS core domain and is more similar to the archaeal type, with an N-terminal Rossmann-fold catalytic domain, an anticodon binding domain, and no extra C-terminal domain. $TyrRS_{apm}$ shares 30% identity over 340 residues with the TyrRS of the hyperthermophilic Euryarchaeota *Pyrococcus horikoshii*, its closest known structural homologue (2CYC [38]).

The protein was cocrystallized with ATP and the tyrosine analogue tyrosinol, and its structure was solved at 2.2-Å resolution. While tyrosinol was clearly located in the electronic density map, only residual density appears at the binding site of ATP, probably due to its instability at the crystallization pH (5.5). We compared the $TyrRS_{apm}$ active site with the *Methanococcus jannaschii* (1J1U [37]) and *Thermus thermophilus* (1H3E [62]) structures in complex with $tRNA^{Tyr}$ and L-tyrosine or tyrosinol and the human TyrRS catalytic core struc-

TABLE 2. Kinetic parameters for tyrosylation of wild-type $tRNA^{Tyr}$ molecules or variants by $TyrRS_{apm}$ and methionylation of wild-type $tRNA^{Met}$ molecules or variants by $MetRS_{apm}$[a]

tRNA	K_m (μM)	k_{cat} (10^{-3} s^{-1})	k_{cat}/K_m (*n*-fold)	*L* value
Tyrosine				
Wild-type molecules				
Yeast (native)	0.5	126	252	0.3
Yeast (transcript)	1.7	142	83.5	1
P. falciparum	4	18.3	4.6	18
Mutated molecules				
Yeast C_1-G_{72}→A_1-U_{72}	NM[b]	NM	NM	NM
Yeast C_1-G_{72}→G_1-C_{72}	NM	NM	NM	NM
Yeast C_1-G_{72}→A_{73}→G_{73}	NM	NM	NM	NM
Yeast G_{34}→A_{34}	1.3	7.5	5.8	14.4
Yeast G_{34}→C_{34}	1.4	9.3	6.6	12.6
Yeast G_{34}→U_{34}	1.3	8.3	6.4	13
Yeast U_{35}→A_{35}	16	2.5	0.16	522
Yeast U_{35}→C_{35}	33.3	10	0.3	278
Yeast U_{35}→G_{35}	9.3	1.1	0.12	696
Yeast A_{36}→G_{36}	20	7.3	0.36	232
Yeast A_{36}→U_{36}	15.4	14.9	0.96	87
Methionine				
Wild-type molecules				
Yeast (native)	0.13	6.6	252	0.3
Yeast (transcript)	0.74	17.4	83.5	1
E. coli (native)	0.47	47	252	0.3
Mutated molecules				
Yeast C_{34}→G_{34}	NM	NM	NM	NM
Yeast A_{35}→C_{35}	NM	NM	NM	NM
Yeast U_{36}→C_{36}	NM	NM	NM	NM

[a] *L* values correspond to losses of efficiency relative to yeast $tRNA^{Tyr}$ transcript or yeast $tRNA^{Met}$ transcript. Values of >1 correspond to gains in efficiency. Experimental errors for k_{cat} and K_m varied at most by 20%. Results represent averages of at least two independent experiments.

[b] NM, not measurable (loss of $>10^5$).

ture (1Q11 [61]) in complex with tyrosinol. The positions of the residues in contact with tyrosinol in the $TyrRS_{apm}$ structure were found to be superimposable to their counterparts in the archaeal structures (Fig. 2) and to correspond to conserved amino acids, except for two histidines replaced by F81 and N198, as in plant and protozoan sequences (Fig. 3).

The ATP binding site of $TyrRS_{apm}$ exhibits a modified version (a HIAQ motif, as in protozoa and plants) of the catalytically important HIGH motif found in the archaeal and eukaryotic structures 1J1U and 1Q11 (Fig. 3). These motifs are superimposable in the structures. A perfect KMSKS motif is present in the $TyrRS_{apm}$ sequence but in an open-state conformation compared to the one observed in 1H3E, the structure of a bacterial TyrRS in complex with tyrosinol and $tRNA^{Tyr}$ (62). This loop, often disordered in ATP-free TyrRS structures, is also associated with large B-factor values in both the $TyrRS_{apm}$ and 1H3E structures.

(ii) Structural peculiarities of the $TyrRS_{apm}$ dimer. In contrast to other tRNA/aaRS systems, where the tRNA binds to a single subunit of the synthetase, the $tRNA^{Tyr}$ recognition involves both TyrRS subunits (6, 62). The acceptor arm of $tRNA^{Tyr}$ interacts with the catalytic domain of one monomer, whereas the anticodon arm is sandwiched between the α-helical and C-terminal domains of the other monomer. In all TyrRS structures, the monomers are related to each other by a twofold rotational axis and the dimers are superimposable, with very small variations in the orientations of the monomers. All available crystal structures of tRNA/TyrRS complexes are also planar, with a symmetrical conformation of the two monomers in the dimer and with two tRNA molecules simultaneously interacting with one TyrRS dimer (62). However, previous kinetic studies of tyrosine activation and $tRNA^{Tyr}$ charging revealed an anticooperative behavior of the TyrRS dimer in solution (27). Other experiments suggested that each TyrRS dimer binds and tyrosylates only one tRNA molecule at a time (7, 20), again putting into question the fact that the symmetrical conformation observed in all crystal structures to date corresponds to the active conformation in solution (62).

Similarly to the other members of the family, $TyrRS_{apm}$ is a dimer in solution (data not shown), and it crystallized as a homodimer. The superimposition of the $TyrRS_{apm}$ structure with all other available TyrRS dimeric structures nonetheless highlights a major difference. While the first monomer super-

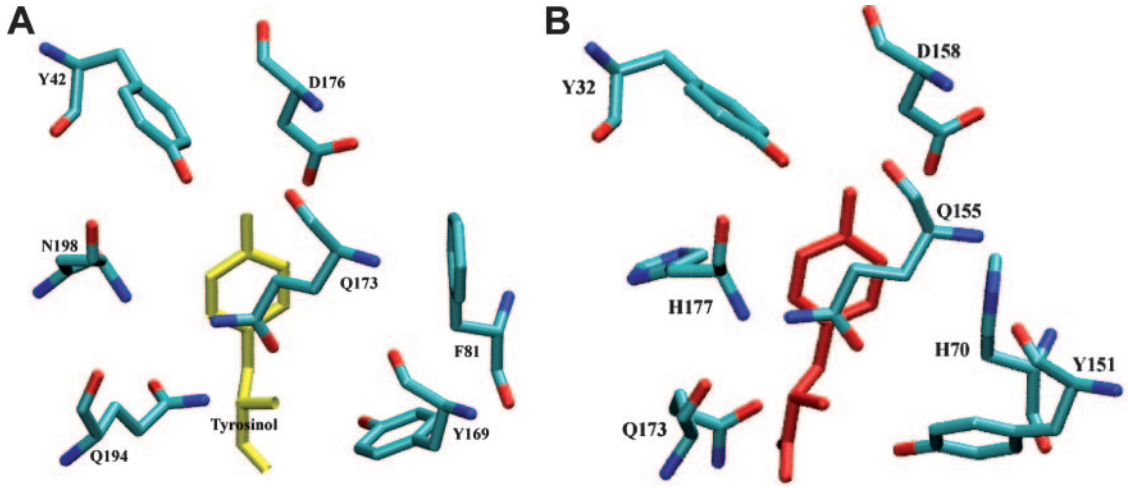

FIG. 2. Invariance of the tyrosinol binding site. Amino acids closest to the tyrosinol molecule (A) in the $TyrRS_{apm}$ and (B) in the *M. jannaschii* TyrRS structures (1J1U).

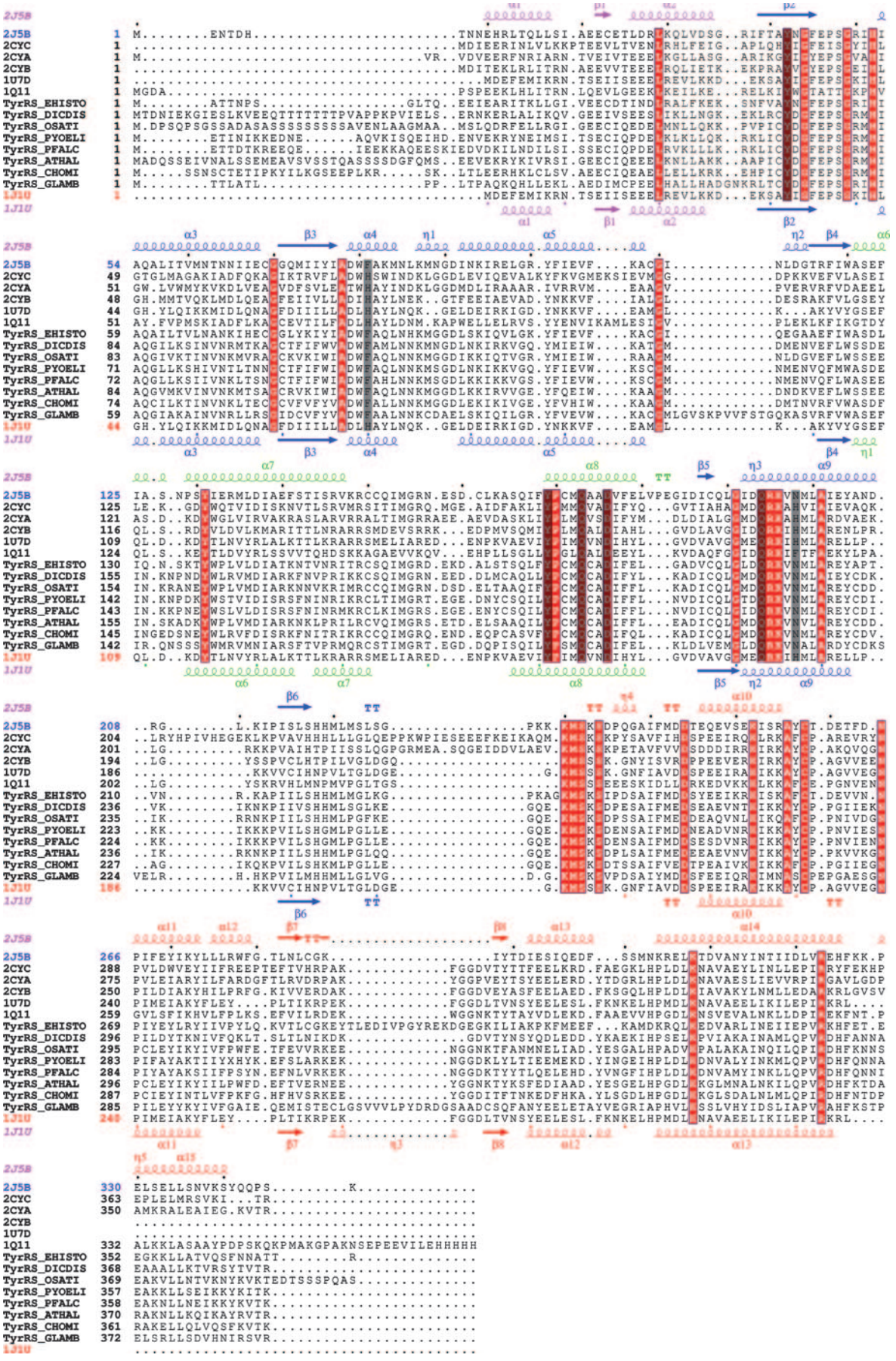

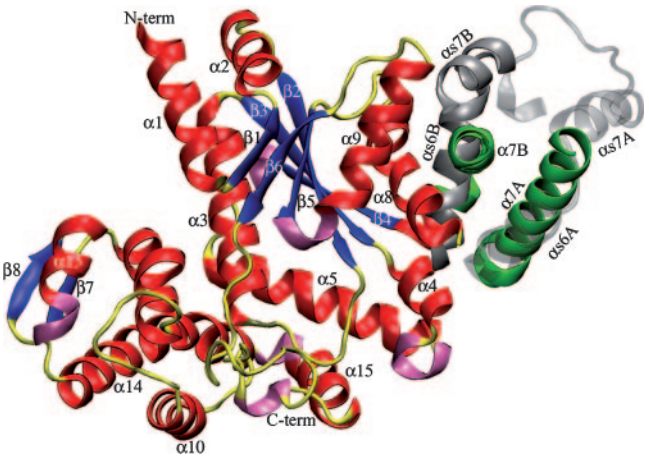

FIG. 4. Cartoon comparison of the dimer interface. The two α7 helices of $TyrRS_{apm}$ are in green, and the conserved αs_6-turn-αs_7 structural motif (found in other TyrRS dimers) is colored in silver, transparent for the first monomer and opaque for the second one. This figure illustrates the nearly 90° rotation of the $TyrRS_{apm}$ second monomer (colored according to secondary-structure elements: red, α-helices; blue, β-strands; yellow, coils and turns; pink, η helices). N-term, N terminus; C-term, C terminus.

imposes very well with the first monomer of other TyrRSs structures (root mean square deviation of <1.6 Å based on Cα superimposition), the second one is found at a nearly 90° angle relative to its position in other dimers (Fig. 4 and 5). Despite this dramatic conformational change, the CP1 domain (Fig. 3) is still central to the $TyrRS_{apm}$ dimer formation as in other TyrRS, but it exhibits a significant alteration of a motif structurally conserved in all other TyrRS structures. This (α_6-turn-α_7) motif, a 14-residue-long helix followed by a 90° turn and a 9-residue-long helix, is now replaced by a 20-residue-long extended helix (α_7) in $TyrRS_{apm}$. This helix is followed by a variable loop disordered in $TyrRS_{apm}$ as well as in the *M. jannaschii* apo TyrRS structure 1U7D. Interestingly, this new and unique conformation of the $TyrRS_{apm}$ dimer is found in two crystal forms ($P2_1$ [2] and $P2_12_12_1$ [this work]).

We investigated how this peculiar structure of the $TyrRS_{apm}$ dimer could be reconciled with the previously proposed model of TyrRS dimer interaction with $tRNA^{Tyr}$. A first possibility is that the conformation of the $TyrRS_{apm}$ dimer, although observed in two crystal forms, is a crystallization artifact. The dimer interface should then appear more flexible than the rest of the molecule, leading to higher B-factor values. This region of the $TyrRS_{apm}$ structure is actually more agitated than its surroundings. However, this is the case for all available TyrRS structures, and this feature is thus not conclusive. We then compared the buried surface areas upon dimer formation for all TyrRS structures. This buried surface value is 2,360 $Å^2$ for $TyrRS_{apm}$ and ranges from 2,970 to 3,300 $Å^2$ for other TyrRSs. Forcing the $TyrRS_{apm}$ dimer into the standard conformation would cost 1,000 $Å^2$ of the buried surface area and greatly reduce its stability. Conversely, forcing the other (canonical) TyrRS dimer into the conformation observed for the $TyrRS_{apm}$ dimer would also be energetically unfavorable, again at a cost of about 1,000 $Å^2$ (see Materials and Methods). Packing forces are thus not likely to be responsible for the unique conformation of the $TyrRS_{apm}$ dimer at odds with the "canonical" TyrRS structures, which sheds new light on the previously observed discrepancies between the enzyme properties in solution versus its crystallographic structure (7, 20, 27).

We then examined the second possibility, namely, that the tRNA could adopt a new position to interact with the observed $TyrRS_{apm}$ dimer. Assuming an invariant structure for the tRNA, we verified that a suitable model of the complex could be built through a rotation of the tRNA relative to the $TyrRS_{apm}$ dimer, as already observed for bacterial tRNA-TyrRS complexes (37). In this crude model, the residues of the $TyrRS_{apm}$ interacting with the acceptor arm of the tRNA are properly positioned, while the anticodon can still be recognized by the anticodon binding site of the second $TyrRS_{apm}$ monomer.

Functional idiosyncrasies of $TyrRS_{apm}$. Wild-type $tRNA^{Tyr}$ from *E. coli* and yeast, in native or transcribed versions, was assayed for tyrosylation by $TyrRS_{apm}$. Both eukaryotic yeast $tRNA^{Tyr}$s (corresponding to TAC and TAT codons) are tyrosylated up to 90%, whereas only a weak activity (>2%) could be detected with *E. coli* $tRNA^{Tyr}$ (Fig. 1C). Kinetic parameters for tyrosylation were slightly altered when comparing the native molecule to the unmodified transcript, resulting in an ~3-fold reduction in aminoacylation efficiency (as defined by the k_{cat}/K_m ratio) (Table 2). These results demonstrate that although the crystallographic dimer does not exhibit the canonical conformation, it is active in solution. Upon interaction with the tRNA, it is thus likely that a productive tRNA/$TyrRS_{apm}$ dimer complex is formed, as discussed previously.

Recognition of the $tRNA^{Tyr}$ acceptor stem: $TyrRS_{apm}$ obeys the identity rules for archea/eukarya. All eukaryal/archaeal $tRNA^{Tyr}$ species possess a C_1-G_{72} base pair located on the top of the acceptor branch that is replaced by the reverse pair in prokaryotic and mitochondrial $tRNA^{Tyr}$ (55). The N_1-N_{72} base pair, part of the tyrosine identity set, also determines the strong phylogenic barrier preventing cross-tyrosylation between eukaryotic $tRNA^{Tyr}$ and bacterial TyrRS (36, 58).

$TyrRS_{apm}$ is active on yeast and inactive on bacterial or mitochondrial $tRNA^{Tyr}$ (data not shown). To assess the conformity of the $TyrRS_{apm}$ to previously defined identity rules,

FIG. 3. Structure-based alignment of TyrRSs. $TyrRS_{apm}$ (2J5B) was aligned with eukaryal (1Q11, human, core structure) and archaeal (2CYC, *P. horikoshii*; 2CYA, *Aeropyrum pernix*; 2CYB, *Archaeoglobus fulgidus*; 1J1U and 1U7D, *M. jannaschii* complex and apo form) structures. The closest $TyrRS_{apm}$ homologues from protozoa and plants are also included (EHISTO, *Entamoeba histolytica*; DICDIS, *Dictyostelium discoideum*; OSATI, *Oryza sativa*; PYOELI, *Plasmodium yoelii*; PFALC, *Plasmodium falciparum*; ATHAL, *Arabidopsis thaliana*; CHOMI, *Cryptosporidium hominis*; GLAMB, *Giardia lamblia*). The secondary-structure elements of $TyrRS_{apm}$ and *M. jannaschii* are, respectively, indicated above and below the multiple alignment. The N-terminal, Rossmann fold, CP1, and C-terminal domains are colored in pink, blue, green, and red, respectively. Strictly conserved residues are boxed in red. Residues involved in tyrosine binding (Fig. 2) are highlighted in gray. This alignment was produced with 3DCoffee (http://www.igs.cnrs-mrs.fr/Tcoffee/tcoffee_cgi/index.cgi) (48), and the figure was produced with ESPript (31).

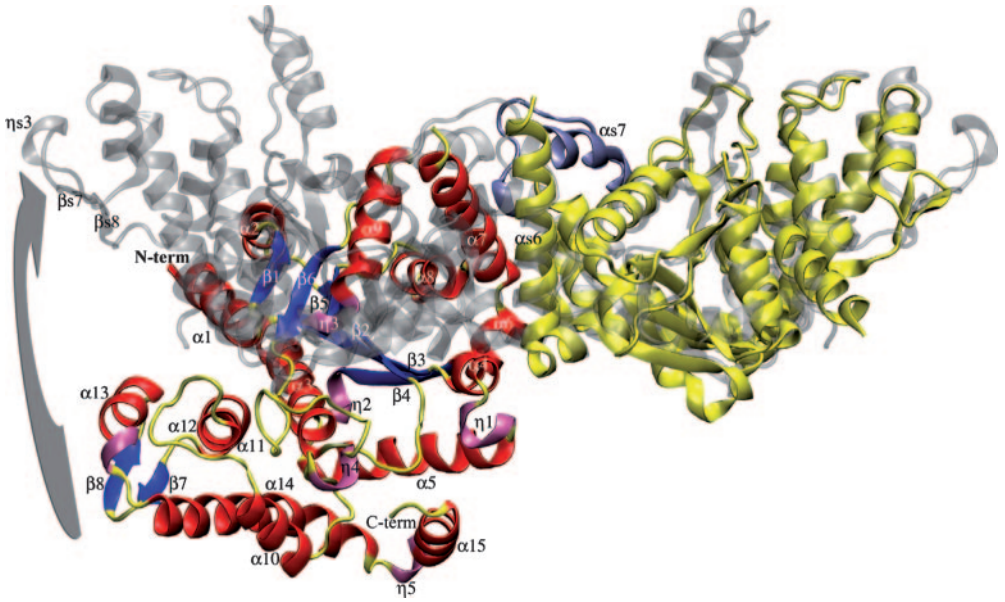

FIG. 5. Cartoon representation of the $TyrRS_{apm}$ dimer superimposed on the archaeal TyrRS 2CYC from *P. horikoshii*. The archaeal dimer is transparent and colored in silver, except for the structural motif (αs_6-turn-αs_7, corresponding to the α_7 helix in $TyrRS_{apm}$), colored in opaque cyan. The $TyrRS_{apm}$ first monomer superimposed on the 1CYC first monomer is colored in yellow. The second monomer secondary-structure elements are colored as outlined in the legend for Fig. 4. The arrow shows the rotation to be applied to the mimivirus second monomer to superimpose its β_7-turn-β_8 onto the *P. horikoshii* βs_7-ηs_3-βs_8 motif. N-term, N terminus; C-term, C terminus.

tyrosylation was assayed on yeast $tRNA^{Tyr}$ transcripts bearing mutations at the following locations: the C_1-G_{72} base pair, the anticodon triplet $G_{34}U_{35}A_{36}$, and the discriminator base A_{73} (26). Replacement of the first base pair by a G_1-C_{72} or an A_1-U_{72} pair inactivates $tRNA^{Tyr}$ tyrosylation by $TyrRS_{apm}$. Similarly, no activity could be detected after mutation of A_{73} into G_{73} (Table 2).

Four synthetase residues are known to be involved in the acceptor stem recognition in archea: R132, R174, K175, and M178 (according to 1J1U numbering). The corresponding amino acids are conserved in $TyrRS_{apm}$ (R149, R195, K196, and M199) (Fig. 3). To analyze their involvement in tRNA binding, we superimposed a $TyrRS_{apm}$ monomer on the monomer of the *M. jannaschii* TyrRS/$tRNA^{Tyr}$ complex at the acceptor site. Except for residue R149, not visible in the $TyrRS_{apm}$ structure, the homologous residues are positioned as in the *M. jannaschii* structure, with residues R195 and M199 contacting the C_1 base and residue K196 contacting the A_{73} discriminator base. In order to make contact with the G_{72} base (as seen with the homologous R132 residue in the *M. jannaschii* TyrRS/$tRNA^{Tyr}$ complex), residue R149 in helix α_7 of the $TyrRS_{apm}$ structure would require a conformational change, breaking the helix into the canonical α_6-turn-α_7 motif. This is consistent with the high B-factor values observed at these positions and the results obtained with the C_1-G_{72}→G_1-C_{72} variant.

Recognition of the $tRNA^{Tyr}$ anticodon. The other residues involved in tyrosine identity correspond to the anticodon nucleotides $G_{34}U_{35}A_{36}$, the strength of which depends on the system studied (9). The two available crystal structures of TyrRS/$tRNA^{Tyr}$ complexes identified the specific contacts established between these identity elements and the amino acid residues on the synthetases (37, 42, 62). By comparison with all available TyrRS sequences and structures, the $TyrRS_{apm}$ loop involved in anticodon recognition is quite short (Fig. 3 and 6). To examine the functional consequence of this unique feature, we studied the tyrosylation of variants derived from yeast $tRNA^{Tyr}$ transcript mutated at anticodon sites. In contrast with the yeast TyrRS, only weak effects were observed upon mutation of the G_{34} anticodon nucleotide (Table 2). The structural comparison of the *M. jannaschii* complex with the $TyrRS_{apm}$ structure highlights that, in the archaeal complex, the G_{34} base is sandwiched between the F261 and H283 rings and is also

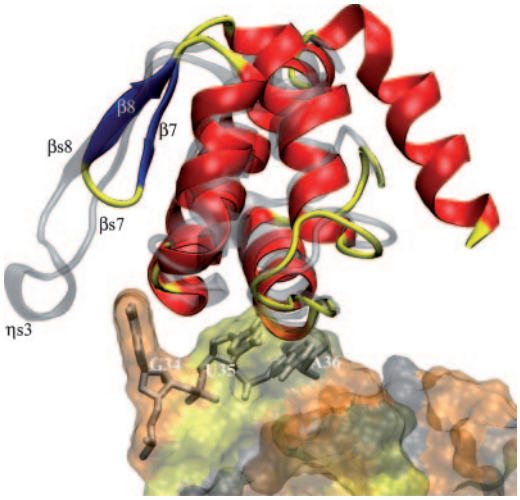

FIG. 6. Superimposition of the C-terminal anticodon binding domain of $TyrRS_{apm}$ (solid) on the *M. jannaschii* TyrRS/tRNA complex (transparent). The anticodon appears solid in the transparent tRNA surface.

recognized by D286 through hydrogen bonds. This part of the $TyrRS_{apm}$ structure exhibits the most significant differences from archaeal/eukaryotic TyrRS. The β-3_{10}-β motif encompassing the F261 position has no counterpart in the mimivirus structure, where it is replaced by a shorter β-turn-β motif, too far away to possibly interact with base G_{34}, on the other side of the anticodon. The H283 and D286 positions are uniquely replaced in the viral sequence by N303 and E306, respectively. Together with our experimental results (Table 2), this suggests that the G_{34} base of the anticodon is not used as a discriminator for $tRNA^{Tyr}$ recognition by $TyrRS_{apm}$.

In contrast, mutations of the two other anticodon nucleotides (nucleotides 35 and 36) induce strong negative effects (from 87- to 696-fold) (Table 2) on the $TyrRS_{apm}$ activity on the corresponding tRNA, which is not observed with the *M. jannaschii* TyrRS, suggesting the viral enzyme specifically recognizes these nucleotides.

Methionylation properties of $MetRS_{apm}$. Wild-type native initiator $tRNA^{Met}$s from *E. coli* and *S. cerevisiae* were tested for methionylation by $MetRS_{apm}$. Both substrates were aminoacylated with kinetic parameters (K_m and k_{cat}) slightly decreased for the eukaryal tRNA, which resulted in a twofold loss in methionylation efficiency compared to that of the *E. coli* $tRNA^{Met}$ (Table 2). Unmodified yeast $tRNA^{Met}$ transcript behaves globally as its native counterpart, with only a twofold loss in aminoacylation efficiency. Noticeable, however, are the low K_m and high k_{cat} values of yeast $tRNA^{Met}$ transcript towards $MetRS_{apm}$ compared to the values determined with the yeast enzyme. Replacing individually the anticodon residues abolishes methionine acceptance (Table 2), as has already been demonstrated for *E. coli* and yeast MetRSs (52, 53). Thus, as for all MetRS, the $C_{34}U_{35}A_{36}$ anticodon residues govern specific recognition of $tRNA^{Met}$ by $MetRS_{apm}$.

Evolutionary origin of $aaRS_{apm}$. Previous functional studies of TyrRSs revealed a phylogenetic barrier preventing cross-tyrosylation of eubacterial $tRNA^{Tyr}$ by eukaryal TyrRS and vice versa (36, 58). Our work demonstrates that $TyrRS_{apm}$ is a bona fide eukaryal enzyme in that respect. This corroborates the sequence alignments revealing homologies of $TyrRS_{apm}$ with eukaryal synthetases (2). Our functional assays of yeast $tRNA^{Tyr}$ transcript variants pointed out additional similarities with the behavior of the yeast enzyme (26), with the C_1-G_{72} base pair and the discriminator nucleotide A_{73} being the strongest identity determinants. The anticodon residues also contribute to the tyrosine identity but to a lesser extent. The largest difference was found for the recognition of base G_{34}, the mutation of which has a strong effect in yeast and other systems (9, 26) but contributes weakly to tyrosylation by $TyrRS_{apm}$.

Two opposite scenarios could account for the presence of four aaRS in the genome of mimivirus. These enzymes, identified in a virus for the first time, could correspond to the remains of an ancestral viral genome that encoded a complete and functional translation apparatus, or they could have been acquired at once or sequentially from ancestral cellular hosts.

The position of mimivirus TyrRS was first analyzed by computing a phylogenetic tree of TyrRS from all domains of life (Fig. 7). The tree robustly separates bacterial and eukaryal TyrRSs on one side from archaeal, protozoan, and plant TyrRSs on the other side. The $TyrRS_{apm}$ sequence is most closely related to TyrRS found in the kingdom Protozoa, and its closest relative is the TyrRS from *Entamoeba histolytica* (54% identical residues over 330 residues). Although amoebas from the genus *Entamoeba* are not hosts to mimivirus (56), they belong to the same Amoebozoa clade as Acanthamoeba (the virus's natural host). In the absence of sequence data for Acanthamoeba TyrRS, we could speculate that the $TyrRS_{apm}$ was actually acquired from an ancestral amoebal host.

However, the TyrRS tree strongly disagrees with the accepted species tree for the Protozoa (3). TyrRSs from reputed distant cellular organisms are found close to each other (e.g., Excavata *Trichomonas* versus Amoebozoa *Entamoeba*, Chromaveolata *Phytophthora* versus Excavata *Trypanosoma*, and Chromaveolata *Plasmodium* versus Amoebozoa *Dictyostelium*), while reputed close organisms are found very distant (e.g., Amoebozoa *Dictyostelium* and *Entamoeba*). The viral $TyrRS_{apm}$ sequence exhibits similar inconsistencies, its next closest homologue belonging to *Trichomonas vaginalis* (52% identical residues), a member of clade Excavata, in principle quite distant from the Amoebozoa supergroup (Fig. 7) (3, 46). At the same time, the sequence of $TyrRS_{apm}$, presumably acquired from an Amoebozoa ancestor host, is only 43% identical to the TyrRS of *Dictyostelium discoideum*, another member of the Amoebozoa. Such inconsistencies suggest that TyrRS genes have been transferred laterally between the ancestors of today's representatives of these various early diverging protozoan clades, thus precluding the unambiguous identification of the source of mimivirus TyrRS or even the direction of an eventual exchange with an Amoebozoa ancestor.

Our experimental results also confirmed the intermediate (ancestral?) status of mimivirus TyrRS. It was found significantly less active (Table 2) on *Plasmodium falciparum* $tRNA^{Tyr}$ transcripts than on yeast $tRNA^{Tyr}$ transcripts, despite a greater sequence similarity between $TyrRS_{apm}$ and *Plasmodium* TyrRS than between $TyrRS_{apm}$ and yeast TyrRS. The difference in activity might be due to the dissimilar D-loop organizations between yeast (member of the Opisthokonta) and *P. falciparum* (member of the Chromalveota) $tRNA^{Tyr}$, as seen in other aminoacylation systems (47).

We extended our phylogenic study to the four mimivirus enzymes by using archeal and eukaryotic aaRS sequences (including bacterial-type mitochondrial eukaryotic aaRS) to investigate their origin. The computed trees (Fig. 8) clearly do not militate in favor of a recent acquisition of any mimivirus aaRS from an amoebal host. Both ArgRS and MetRS exhibit a basal branching, predating the radiation of the eukaryotic kingdom and of most protozoan supergroups (3). In contrast, mimivirus CysRS exhibits a strong affinity with the Excavata member *Giardia lamblia*. However, like the previous TyrRS tree (Fig. 7 and 8) these trees exhibit serious inconsistencies with the accepted protozoan species tree, again suggesting an active lateral exchange of these genes among early diverging protozoan ancestors. Altogether, these results argue against a recent acquisition of these aaRS by the mimivirus lineage and are not incompatible with their presence in a mimivirus ancestor genome prior to the divergence of the various protozoan supergroups.

If the evolutionary origin of $TyrRS_{apm}$, remains ambiguous,

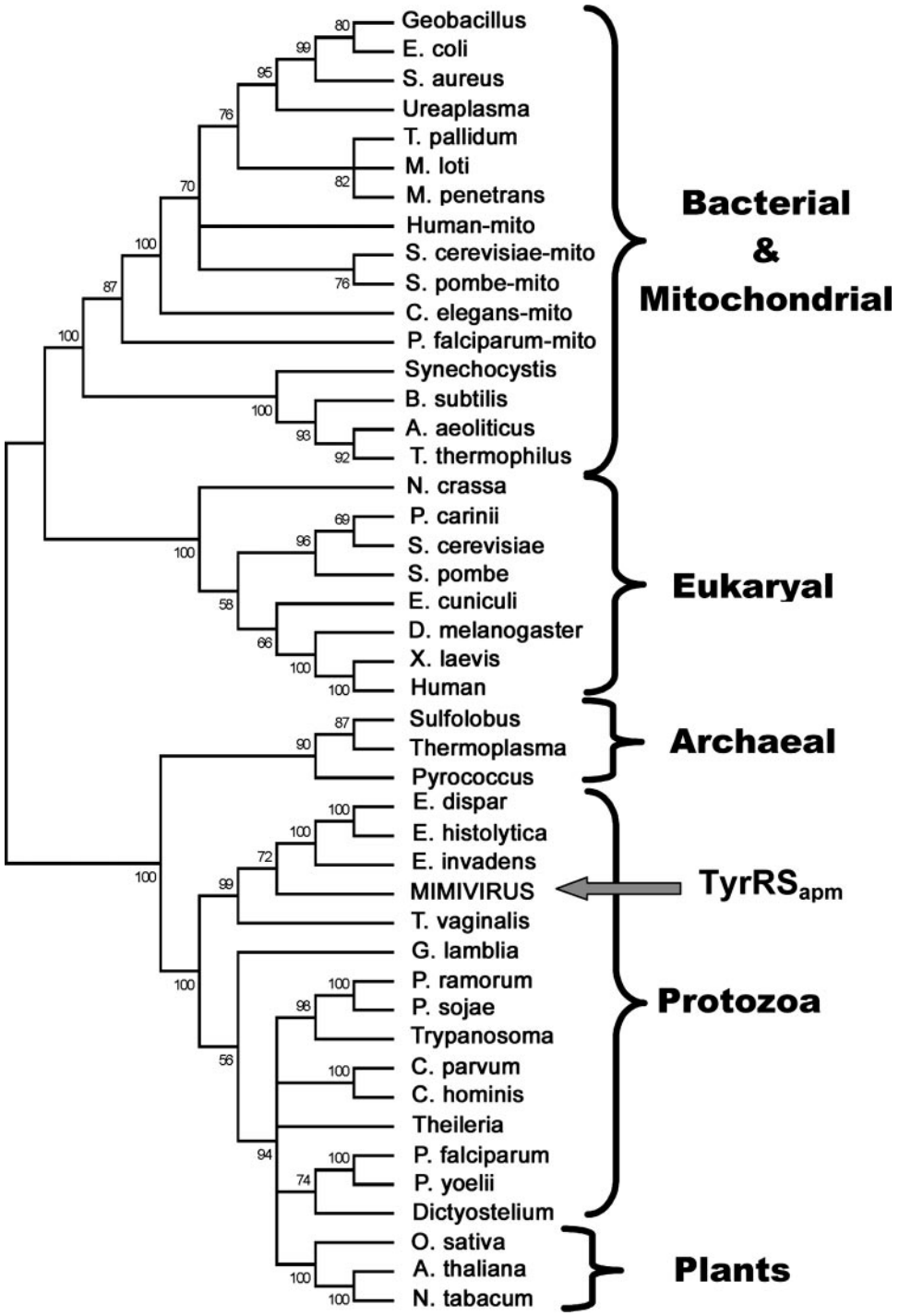

FIG. 7. Phylogenetic position of mimivirus TyrRS. *S. aureus*, *Staphylococcus aureus*; *T. pallidum*, *Treponema pallidum*; *M. loti*, *Mesorhizobium loti*; *M. penetrans*, *Mycoplasma penetrans*; *S. pombe*, *Schizosaccharomyces pombe*; *C. elegans*, *Caenorhabditis elegans*; *B. subtilis*, *Bacillus subtilis*; *A. aeoliticus*, *Aquifex aeoliticus*; *P. carinii*, *Pneumocystis carinii*; *E. cuniculi*, *Encephalitozoon cuniculi*; *D. melanogaster*, *Drosophila melanogaster*; *X. laevis*, *Xenopus laevis*; *E. dispar*, *Entamoeba dispar*; *E. invadens*, *Entamoeba invadens*; *P. ramorum*, *Phytophthora ramorum*; *P. sojae*, *Phytophthora sojae*; *C. parvum*, *Cryptosporidium parvum*; *C. hominis*, *Cryptosporidium hominis*; *P. yoelii*, *Plasmodium yoelii*; *O. sativa*, *Oryza sativa*; *A. thaliana*, *Arabidopsis thaliana*; *N. tabacum*, *Nicotiana tabacum*. All other organisms are defined in the text. mito, mitochondrial sequences.

the specificity of its activity, its structure, and its phylogenetic position classify it as a typical archaeal/eukaryotic TyrRS in a protozoan lineage closer to the archaeal lineage than to the one encompassing the cytoplasmic metazoan and yeast TyrRSs (Fig. 8). Its short sequence and its good specific activity are reminiscent of the concept of "optimized" viral enzymes already proposed in the context of other large DNA viruses (60). The lack of recognition of the third anticodon nucleotide by

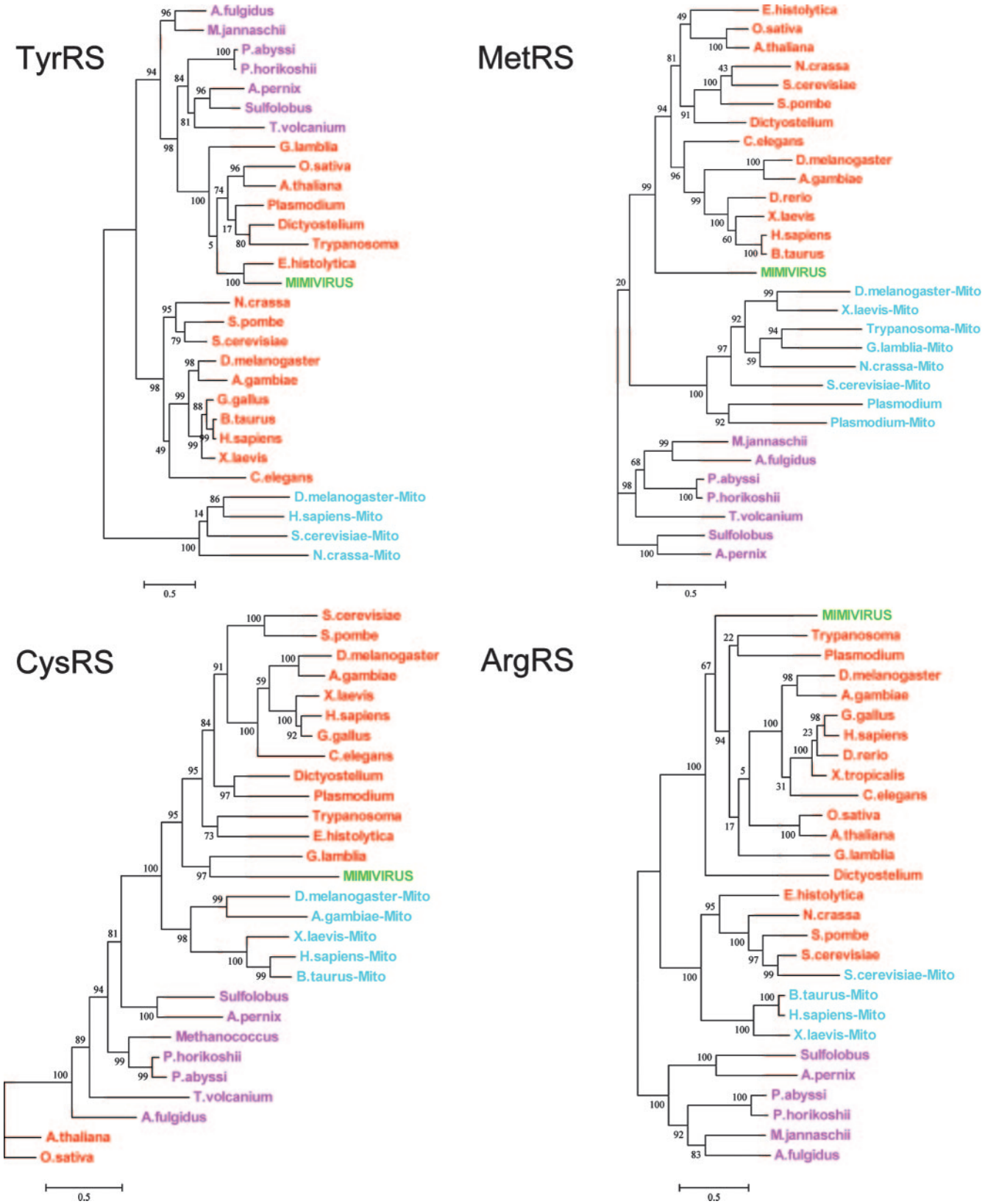

FIG. 8. Phylogenetic position of mimivirus aaRS. Archeal sequences are colored in purple, eukaryotic in red, mitochondrial (Mito) (bacterial type) in cyan, and mimivirus in green. *A. fulgidus*, *Archaeoglobus fulgidus*; *P. abyssi*, *Pyrococcus abyssi*; *A. pernix*, *Aeropyrum pernix*; *T. volcanium*, *Thermoplasma volcanium*; *A. gambiae*, *Anopheles gambiae*; *G. gallus*, *Gallus gallus*; *B. taurus*, *Bos taurus*; *H. sapiens*, *Homo sapiens*; *D. rerio*, *Danio rerio*; *X. tropicalis*, *Xenopus tropicalis*. All other organisms are defined in the text or the legend for Fig. 7.

$TyrRS_{apm}$ might be either a simplification made possible by the absence of tRNA for TAG and TAA codons or, more boldly, a reminiscence of an ancestral two-letter genetic code. Future biochemical and structural studies on the other mimivirus aaRS might help to answer these questions.

Conclusions. The discovery of four aaRS in the genome of mimivirus, together with other proteins central to the translation apparatus (initiation factor, elongation factor, peptide release factors, and tRNA modification enzyme) (49), violated the established view that protein translation is a process uniquely encoded by cellular organisms. Still, mimivirus possesses only a few of all of the genes necessary to encode a functional protein translation apparatus, and the presence of only four aaRS (together with six tRNAs, five of which are substrates of other aaRS) does not make immediate biochemical sense. Yet, the presence of tRNAs in DNA virus genomes is not uncommon, in particular in large phycodnaviruses (to date, the closest lineage to Mimiviridae [15]), where some of them participate directly in the translation process (60). Sequenced chlorella virus genomes also exhibit a homologue of the fungal-specific translation elongation factor 3 (e.g., open reading frame A666L in *Paramecium bursaria* chlorella virus type 1 [57]), most similar to a chlorella homologue, strongly suggesting (in contrast with mimivirus aaRS) a recent horizontal transfer with an ancestor of today's chlorovirus hosts (data not shown).

In the absence of an obvious reason for cellular-specific functions found to be encoded by viruses, the traditional interpretation is that they correspond to a regulatory function helping the virus hijack the cell metabolism. A number of accessory roles have been described for synthetases. For instance, two aaRS (including the mitochondrial TyrRS of *Neurospora crassa*) have been involved in splicing of group I introns (14, 41). Eukaryotic aaRS have also been involved in cell cycle control (36, 59), the direct biosynthesis of pyrrolysine and selenocysteine, and the regulation of the pool of cytoplasmic/nuclear tRNA (reviewed in reference 28). More recently, the yeast AspRS has been shown to regulate its expression by interacting with its own mRNA (29). Noticeably, these accessory functions all require the presence of special features or domains not found in mimivirus aaRS. None of these functions have yet been described in the context of virus infections.

Rather unexpectedly, our structural and functional analysis of the two viral $aaRS_{apm}$ did not reveal any unusual features that might suggest involvement in nonenzymatic, accessory processes. On the contrary, the structure of $TyrRS_{apm}$ corresponds to the minimal archaeal-like core catalytic domain, is indeed specific of tyrosine, and obeys the expected rules of interaction with eukaryal cognate tRNAs. $MetRS_{apm}$ is also specific for methionine and behaves as a regular eukaryotic MetRS. According to these results, the most parsimonious explanation remains that mimivirus $aaRS_{apm}$ directly participates in the protein translation process in infected cells. Further experiments are required to determine how essential these virus-encoded aaRS are to mimivirus replication and how they complement or interfere with the amoeba translation machinery.

ACKNOWLEDGMENTS

We are grateful to D. Raoult for providing the mimivirus genomic DNA and to Gérard Keith and Franco Fasiolo (IBMC, Strasbourg, France) for the generous gifts of yeast initiator $tRNA^{Met}$ and $tRNA^{Met}$ clones, respectively. We also thank D. Nurizzo for data collection at ESRF on ID29 beamline; Y. Ogata, S. Chenivesse, and D. Byrne for technical assistance; A. Lartigue for helpful discussions; and P. Hingamp for reading the manuscript. We acknowledge the use of the Marseille-Nice Génopole bioinformatic platform.

This work was supported by Centre National de la Recherche Scientifique (CNRS), Université Louis Pasteur, Strasbourg, and the French Ministry for Research (ACI BCMS).

REFERENCES

1. **Abergel, C., B. Coutard, D. Byrne, S. Chenivesse, J. B. Claude, C. Deregnaucourt, T. Fricaux, C. Gianesini-Boutreux, S. Jeudy, R. Lebrun, C. Maza, C. Notredame, O. Poirot, K. Suhre, M. Varagnol, and J.-M. Claverie.** 2003. Structural genomics of highly conserved microbial genes of unknown function in search of new antibacterial targets. J. Struct. Funct. Genomics **4:**141–157.
2. **Abergel, C., S. Chenivesse, D. Byrne, K. Suhre, V. Arondel, and J.-M. Claverie.** 2005. Mimivirus TyrRS: preliminary structural and functional characterization of the first amino-acyl tRNA synthetase found in a virus. Acta Crystallogr. F **61:**212–215.
3. **Adl, S. M., A. G. Simpson, M. A. Farmer, R. A. Andersen, O. R. Anderson, J. R. Barta, S. S. Bowser, G. Brugerolle, R. A. Fensome, S. Fredericq, T. Y. James, S. Karpov, P. Kugrens, J. Krug, C. E. Lane, L. A. Lewis, J. Lodge, D. H. Lynn, D. G. Mann, R. M. McCourt, L. Mendoza, O. Moestrup, S. E. Mozley-Standridge, T. A. Nerad, C. A. Shearer, A. V. Smirnov, F. W. Spiegel, and M. F. Taylor.** 2005. The new higher level classification of eukaryotes with emphasis on the taxonomy of protists. J. Eukaryot. Microbiol. **52:**399–451.
4. **Aphasizhev, R., A. Théobald-Dietrich, D. Kostyuk, S. N. Kochetkov, L. Kisselev, R. Giegé, and F. Fasiolo.** 1997. Structure and aminoacylation capacities of tRNA transcripts containing deoxyribonucleotides. RNA **3:**893–904.
5. **Arnez, J. G., and D. Moras.** 1997. Structural and functional considerations of the aminoacylation reaction. Trends Biochem. Sci. **22:**211–216.
6. **Bedouelle, H., and G. Winter.** 1986. A model of synthetase/transfer RNA interaction as deduced by protein engineering. Nature **320:**371–373.
7. **Bedouelle, H.** 1990. Recognition of tRNAtyr by tyrosyl-tRNA synthetase. Biochimie **72:**589–598.
8. **Bedouelle, H.** 2005. Tyrosyl-tRNA synthetases, p. 111–124. *In* M. Ibba, C. Francklyn, and S. Cusack (ed.), Aminoacyl-tRNA synthetases. Landes Biosciences, Georgetown, TX.
9. **Bonnefond, L., R. Giegé, and J. Rudinger-Thirion.** 2005. Evolution of the $tRNA^{Tyr}$/TyrRS aminoacylation systems. Biochimie **87:**873–883.
10. **Bricogne, G., C. Vonrhein, C. Flensburg, M. Schiltz, and W. Paciorek.** 2003. Generation, representation and flow of phase information in structure determination: recent developments in and around SHARP 2.0. Acta Crystallogr. D **59:**2023–2030.
11. **Brunger, A. T., P. D. Adams, G. M. Clore, W. L. DeLano, P. Gros, R. W. Grosse-Kunstleve, J. S. Jiang, J. Kuszewski, M. Nilges, N. S. Pannu, R. J. Read, L. M. Rice, T. Simonson, and G. L. Warren.** 1998. Crystallography and NMR system: a new software suite for macromolecular structure determination. Acta Crystallograph. D **54:**905–921.
12. **Campanacci, V., D. Y. Dubois, H. D. Becker, D. Kern, S. Spinelli, C. Valencia, F. Pagot, A. Salomoni, S. Grisel, R. Vincentelli, C. Bignon, J. Lapointe, R. Giegé, and C. Cambillau.** 2004. The Escherichia coli YadB gene product reveals a novel aminoacyl-tRNA synthetase like activity. J. Mol. Biol. **337:**273–283.
13. **Carter, C. W., Jr.** 1993. Cognition, mechanism, and evolutionary relationships in aminoacyl-tRNA synthetases. Annu. Rev. Biochem. **62:**715–748.
14. **Cherniack, A. D., G. Garriga, J. D. Kittle, Jr., R. A. Akins, and A. M. Lambowitz.** 1990. Function of Neurospora mitochondrial tyrosyl-tRNA synthetase in RNA splicing requires an idiosyncratic domain not found in other synthetase. Cell **62:**745–755.
15. **Claverie, J.-M., H. Ogata, S. Audic, C. Abergel, K. Suhre, and P.-E. Fournier.** 2006. Mimivirus and the emerging concept of giant virus. Virus Res. **117:**133–144.
16. **Collaborative Computational Project Number 4.** 1994. The CCP4 suite: programs for protein crystallography. Acta Crystallogr. D **50:**760–763.
17. **Cusack, S., C. Berthet-Colominas, M. Härtlein, N. Nassar, and R. Leberman.** 1990. A second class of synthetase structure revealed by X-ray analysis of *Escherichia coli* seryl-tRNA synthetase at 2.5 Å. Nature **347:**249–255.
18. **Delarue, M., and D. Moras.** 1993. The aminoacyl-tRNA synthetases family: modules at work. Bioessays **15:**675–687.
19. **Despons, L., B. Senger, F. Fasiolo, and P. Walter.** 1992. The anticodon triplet is not sufficient to confer methionine acceptance to a transfer RNA. J. Mol. Biol. **225:**897–907.
20. **Dessen, P., G. Zaccaï, and S. Blanquet.** 1982. Neutron scattering studies of

Escherichia coli tyrosyl-tRNA synthetase and of its interaction with tRNA-tyr. J. Mol. Biol. **159:**651–664.
21. **Dirheimer, G., and J.-P. Ebel.** 1967. Fractionation of Brewer's yeast t-RNA by countercurrent distribution. Bull. Soc. Chim. Biol. (Paris) **49:**1679–1687.
22. **Edgar, R. C.** 2004. MUSCLE: a multiple sequence alignment method with reduced time and space complexity. BMC Bioinformatics **5:**113.
23. **Eriani, G., M. Delarue, O. Poch, J. Gangloff, and D. Moras.** 1990. Partition of tRNA synthetases into two classes based on mutually exclusive sets of sequence motifs. Nature **347:**203–206.
24. **Evans, P. R.** 1993. Data reduction, p. 114–122. *In* L. Sawyer, N. Isaacs, and S. Bailey (ed)., Proceedings of CCP4 Study Weekend, on data collection and processing. Daresbury Laboratory, Warrington, United Kingdom.
25. **Fechter, P., J. Rudinger, R. Giegé, and A. Théobald-Dietrich.** 1998. Ribozyme processed tRNA transcripts with unfriendly internal promoter for T7 RNA polymerase: production and activity. FEBS Lett. **436:**99–103.
26. **Fechter, P., J. Rudinger-Thirion, A. Théobald-Dietrich, and R. Giegé.** 2000. Specific tyrosylation of the bulky tRNA-like structure of Brome mosaic virus RNA relies solely on identity nucleotides present in its amino acid accepting domain. Biochemistry **39:**1725–1733.
27. **Fersht, A. R., and R. Jakes.** 1975. Tyrosyl-tRNA synthetase from Escherichia coli. Stoichiometry of ligand binding and half-of-the-sites reactivity in aminoacylation. Biochemistry **14:**3344–3350.
28. **Francklyn, C., J. J. Perona, J. Puetz, and Y. M. Hou.** 2002. Aminoacyl-tRNA synthetases: versatile players in the changing theater of translation. RNA **8:**1363–1372.
29. **Frugier, M., M. Ryckelynck, and R. Giegé.** 2005. tRNA-balanced expression of a eukaryal aminoacyl-tRNA synthetase by an mRNA-mediated pathway. EMBO Rep. **6:**860–865.
30. **Giegé, R., M. Sissler, and C. Florentz.** 1998. Universal rules and idiosyncratic features in tRNA identity. Nucleic Acids Res. **26:**5017–5035.
31. **Gouet, P., E. Courcelle, D. I. Stuart, and F. Metoz.** 1999. ESPript: multiple sequence alignments in PostScript. Bioinformatics **15:**305–308.
32. **Guindon, S., and O. Gascuel.** 2003. A simple, fast, and accurate algorithm to estimate large phylogenies by maximum likelihood. Syst. Biol. **52:**696–704.
33. **Hartley, J. L., G. F. Temple, and M. A. Brasch.** 2000. DNA cloning using in vitro site-specific recombination. Genome Res. **10:**1788–1795.
34. **Hendrickson, W. A., J. R. Horton, and D. M. LeMaster.** 1990. Selenomethionyl proteins produced for analysis by multiwavelength anomalous diffraction (MAD): a vehicle for direct determination of three-dimensional structure. EMBO J. **9:**1665–1672.
35. **Humphrey, W., A. Dalke, and K. Schulten.** 1996. VMD—visual molecular dynamics. J. Mol. Graphics **14:**33–38.
36. **Kleeman, T. A., D. Wei, K. L. Simpson, and E. A. First.** 1997. Human tyrosyl-tRNA synthetase shares amino acid sequence homology with a putative cytokine. J. Biol. Chem. **272:**14420–14425.
37. **Kobayashi, T., O. Nureki, R. Ishitani, A. Yaremchuk, M. Tukalo, S. Cusack, K. Sakamoto, and S. Yokoyama.** 2003. Structural basis for orthogonal tRNA specificities of tyrosyl-tRNA synthetases for genetic code expansion. Nat. Struct. Biol. **10:**425–432.
38. **Kuratani, M., H. Sakai, M. Takahashi, T. Yanagisawa, T. Kobayashi, K. Murayama, L. Chen, Z. J. Liu, B. C. Wang, C. Kuroishi, S. Kuramitsu, T. Terada, Y. Bessho, M. Shirouzu, S. Sekine, and S. Yokoyama.** 2006. Crystal structures of tyrosyl-tRNA synthetases from Archaea. J. Mol. Biol. **355:**395–408.
39. **Laskowski, R. A., M. W. MacArthur, D. S. Moss, and J. M. Thornton.** 1993. PROCHECK: a program to check the stereochemical quality of protein structures. J. Appl. Crystallogr. **26:**283–291.
40. **Leslie, A.** 1993. Auto indexing of rotation diffraction images and parameter refinement, p. 44–51. *In* L. Sawyer, N. Issacs, and S. Bailey (ed.), Proceedings of CCP4 Study Weekend, on data collection and processing. Daresbury Laboratory, Warrington, United Kingdom.
41. **Myers, C. A., B. Kuhla, S. Cusack, and A. M. Lambowitz.** 2002. tRNA-like recognition of group I introns by a tyrosyl-tRNA synthetase. Proc. Natl. Acad. Sci. USA **99:**2630–2635.
42. **Nair, S., L. Ribas de Pouplana, F. Houman, A. Avruch, X. Shen, and P. Schimmel.** 1997. Species-specific tRNA recognition in relation to tRNA synthetase contact residues. J. Mol. Biol. **269:**1–9.
43. **Navaza, J.** 2001. Implementation of molecular replacement in AMoRe. Acta Crystallogr. D **57:**1367–1372.
44. **Nicholls, A., K. A. Sharp, and B. Honig.** 1991. Protein folding and association: insights from the interfacial and thermodynamic properties of hydrocarbons. Proteins Struct. Funct. Genet. **11:**281–296.
45. **Notredame, C., D. Higgins, and J. Heringa.** 2000. T-Coffee: a novel method for multiple sequence alignments. J. Mol. Biol. **302:**205–217.
46. **Ogata, H., C. Abergel, D. Raoult, and J.-M. Claverie.** 2005. Response to comment on the 1.2-megabase genome sequence of mimivirus. Science **308:**1114.
47. **Perret, V., C. Florentz, J. D. Puglisi, and R. Giegé.** 1992. Effect of conformational features on the aminoacylation of tRNAs and consequences on the permutation of tRNA specificities. J. Mol. Biol. **226:**323–333.
48. **Poirot, O., K. Suhre, C. Abergel, E. O'Toole, and C. Notredame.** 2004. 3DCoffee@igs: a web server for combining sequences and structures into a multiple sequence alignment. Nucleic Acids Res. **32:**W37–W40.
49. **Raoult, D., S. Audic, C. Robert, C. Abergel, P. Renesto, H. Ogata, B. La Scola, M. Suzan, and J.-M. Claverie.** 2004. The 1.2-Mb genome sequence of Mimivirus. Science **306:**1344–1350.
50. **Roussel, A., and C. Cambillau.** 1991. TURBO-FRODO in silicon graphics geometry partners directory. Silicon Graphics, Mountain View, CA.
51. **Sali, A., and T. L. Blundell.** 1993. Comparative protein modelling by satisfaction of spatial restraints. J. Mol. Biol. **234:**779–815.
52. **Schulman, L. H., and H. Pelka.** 1988. Anticodon switching changes the identity of methionine and valine transfer RNAs. Science **242:**765–768.
53. **Senger, B., and F. Fasiolo.** 1996. Yeast tRNAMet recognition by methionyl-tRNA synthetase requires determinants from the primary, secondary and tertiary structure: a review. Biochimie **78:**597–604.
54. **Sohm, B., M. Frugier, H. Brulé, K. Olszak, A. Przykorska, and C. Florentz.** 2003. Towards understanding human mitochondrial leucine aminoacylation identity. J. Mol. Biol. **328:**995–1010.
55. **Sprinzl, M., and K. S. Vassilenko.** 2005. Compilation of tRNA sequences and sequences of tRNA genes. Nucleic Acids Res. **33:**D139–D140.
56. **Suzan-Monti, M., B. La Scola, and D. Raoult.** 2006. Genomic and evolutionary aspects of Mimivirus. Virus Res. **117:**145–155.
57. **Van Etten, J. L., M. V. Graves, D. G. Müller, W. Boland, and N. Delaroque.** 2002. *Phycodnaviridae*—large DNA algal viruses. Arch. Virol. **147:**1479–1516.
58. **Wakasugi, K., C. L. Quinn, N. Tao, and P. Schimmel.** 1998. Genetic code in evolution: switching species-specific aminoacylation with a peptide transplant. EMBO J. **17:**297–305.
59. **Wakasugi, K., and P. Schimmel.** 1999. Two distinct cytokines released from a human aminoacyl-tRNA synthetase. Science **284:**147–150.
60. **Yamada, T., H. Onimatsu, and J. L. Van Etten.** 2006. Chlorella viruses. Adv. Virus Res. **66:**293–336.
61. **Yang, X. L., F. J. Otero, R. J. Skene, D. E. McRee, P. Schimmel, and L. Ribas de Pouplana.** 2003. Crystal structures that suggest late development of genetic code components for differentiating aromatic side chains. Proc. Natl. Acad. Sci. USA **100:**15376–15380.
62. **Yaremchuk, A., I. Kriklivyi, M. Tukalo, and S. Cusack.** 2002. Class I tyrosyl-tRNA synthetase has a class II mode of cognate tRNA recognition. EMBO J. **21:**3829–3840.